Effects of Thermal Processes on the Structure of Monolithic Tungsten and Tungsten Alloy Photonic Crystals

Nicholas R. Denny,[†] Sang Eon Han,[‡] David J. Norris,[‡] and Andreas Stein*[,†]

Department of Chemistry, University of Minnesota, 207 Pleasant Street Southeast, Minneapolis, Minnesota 55455, and Department of Chemical Engineering & Materials Science, University of Minnesota, 421 Washington Avenue, Minneapolis, Minnesota 55455

Received May 7, 2007. Revised Manuscript Received July 2, 2007

Monolithic pieces of tungsten inverse opals with millimeter dimensions were synthesized by infiltration of poly(methyl methacrylate) colloidal crystals with the aqueous tungsten precursors, acetylated peroxotungstic acid or ammonium metatungstate hydrate. Reduction in hydrogen removed the polymer spheres and formed a very open tungsten skeleton with periodic structure (325−363 nm macropores) and very different morphologies from the surface-templated structures usually obtained by tungsten CVD methods. When these tungsten photonic crystals were resistively or radiatively heated in a nitrogen atmosphere that was not completely dry, tungsten needles formed by chemical vapor transport. More rigorous exclusion of water eliminated the growth of needles, but significant grain growth diminished the structural integrity of the photonic crystal. By doping tungsten with ca. 3 wt % molybdenum, grain growth could be significantly reduced and needle formation eliminated, even in atmospheres that were not completely dry.

Introduction

Photonic crystals—three-dimensionally periodic structures on an optical length scale—have been investigated widely because of their abilities to confine and control light.[1−7] Whereas most studies of photonic crystals have involved dielectric or metal−dielectric compositions, interest has grown in metallic photonic crystals because of their ability to manipulate thermal emission. Lin et al. demonstrated for a tungsten woodpile structure that thermal emission of the heated photonic crystal was modified and, in particular, emission at certain infrared wavelengths was suppressed.[8,9] Thus, metallic photonic crystals show potential for generating infrared radiation in narrow spectral ranges, reducing undesirable heat from a material, and improving the efficiency of emission sources, thermo-photovoltaic systems, and chemical sensors.[10]

The tungsten woodpile structure was prepared by CVD of tungsten within a silica template that was fabricated by a complex layer-by-layer growth technique requiring repetitive deposition and etching of multiple dielectric films.[11] An alternate approach to tungsten photonic crystals involves colloidal crystal templates, which are prepared by simpler natural assembly techniques.[12−30] Using colloidal crystals of

* Corresponding author. Phone: (612) 624-1802. Fax: (612) 626-7541. E-mail: stein@chem.umn.edu.

[†] Department of Chemistry, University of Minnesota.

[‡] Department of Chemical Engineering & Materials Science, University of Minnesota.

(1) John, S. *Phys. Rev. Lett.* **1987**, *58*, 2486−2489.
(2) Yablonovitch, E. *Phys. Rev. Lett.* **1987**, *58*, 2059−2062.
(3) Joannopoulos, J. D.; Villeneuve, P. R.; Fan, S. *Nature* **1997**, *386*, 143−149.
(4) Yablonovitch, E. *Sci. Am.* **2001**, *285*, 34−41.
(5) Soukoulis, C. M. *Photonic Crystals and Light Localization*; Kluwer: Dordrecht, The Netherlands, 2001.
(6) Polman, A.; Wiltzius, P. *MRS Bull.* **2001**, *26*, 608−610.
(7) López, C. *Adv. Mater.* **2003**, *15*, 1679−1704.
(8) Fleming, J. G.; Lin, S. Y.; El-Kady, I.; Biswas, R.; Ho, K. M. *Nature* **2002**, *417*, 52−55.
(9) Lin, S. Y.; Moreno, J.; Fleming, J. G. *Appl. Phys. Lett* **2003**, *83*, 380−382.
(10) Yu, X.; Lee, Y. J.; Furstenberg, R.; White, J. O.; Braun, P. V. *Adv. Mater.* **2007**, *19*, 1689−1692.
(11) Lin, S. Y.; Fleming, J. G.; Hetherington, D. L.; Smith, B. K.; Biswas, R.; Ho, K. M.; Sigalas, M. M.; Zubrzycki, W.; Kurtz, S. R.; Bur, J. *Nature* **1998**, *394*, 251−253.
(12) Xia, Y.; Gates, B.; Li, Z. Y. *Adv. Mater.* **2001**, *13*, 409−413.
(13) Lytle, J. C.; Stein, A. Recent Progress in Syntheses and Applications of Inverse Opals and Related Macroporous Materials Prepared by Colloidal Crystal Templating. In *Annual Reviews of Nano Research*; Cao, G., Brinker, C. J. Eds.; World Scientific Publishing Co.: Hackensack, NJ, 2007; Vol. 1, pp 1−79.
(14) Stein, A.; Schroden, R. C. *Curr. Opin. Solid State Mater. Sci.* **2001**, *5*, 553−564 and references therein.
(15) Kulinowski, K. M.; Jiang, P.; Vaswani, H.; Colvin, V. L. *Adv. Mater.* **2000**, *12*, 833−838.
(16) Velev, O. D.; Tessier, P. M.; Lenhoff, A. M.; Kaler, E. W. *Nature* **1999**, *401*, 548.
(17) Tessier, P. M.; Velev, O. D.; Kalambur, A. T.; Rabolt, J. F.; Lenhoff, A. M.; Kaler, E. W. *J. Am. Chem. Soc.* **2000**, *122*, 9554−9555.
(18) Tessier, P. M.; Velev, O. D.; Kalambur, A. T.; Lenhoff, A. M.; Rabolt, J. F.; Kaler, E. W. *Adv. Mater.* **2001**, *13*, 396−400.
(19) Egan, G. L.; Yu, J. S.; Kim, C. H.; Lee, S. J.; Schaak, R. E.; Mallouk, T. E. *Adv. Mater.* **2000**, *12*, 1040−1042.
(20) Yan, H.; Blanford, C. F.; Holland, B. T.; Parent, M.; Smyrl, W. H.; Stein, A. *Adv. Mater.* **1999**, *11*, 1003−1006.
(21) Yan, H.; Blanford, C. F.; Smyrl, W. H.; Stein, A. *Chem. Commun.* **2000**, 1477−1478.
(22) Yan, H.; Blanford, C. F.; Lytle, J. C.; Carter, C. B.; Smyrl, W. H.; Stein, A. *Chem. Mater.* **2001**, *13*, 4314−4321.
(23) Wijnhoven, J. E. G. J.; Zenvenhuizen, S. J. M.; Hendriks, M. A.; Vanmaekelbergh, D.; Kelly, J. J.; Vos, W. L. *Adv. Mater.* **2000**, *12*, 888−890.
(24) Xu, L.; Zhou, W. L.; Frommen, C.; Baughman, R. H.; Zakhidov, A. A.; Malkinski, L.; Wang, J. Q.; Wiley, J. B. *Chem. Commun.* **2000**, 997−998.
(25) Luo, Q.; Liu, Z.; Li, L.; Xie, S.; Kong, J.; Zhao, D. *Adv. Mater.* **2001**, *13*, 286−289.
(26) Sumida, T.; Wada, Y.; Kitamura, T.; Yanagida, S. *Langmuir* **2002**, *18*, 3886−3894.
(27) Bartlett, P. N.; Birkin, P. R.; Ghanem, M. A. *Chem. Commun.* **2000**, 1671−1672.

10.1021/cm071228p CCC: $37.00
Published on Web 08/15/2007

uniform silica spheres as templates, Ozin and co-workers produced a tungsten inverse opal structure by CVD of tungsten hexacarbonyl.[31] Through this approach, arrays of hollow tungsten spheres with small windows were obtained, especially at higher levels of metal infiltration. Strong absorption in the visible spectral region resulted in a breakdown of the photonic band structure, first in a sphere-cavity-like behavior and, at increased loadings, in a behavior akin to that of a periodically structured metal surface.[31] If the propagating light is absorbed before it can interact with the periodic structure, the influence of the photonic crystal is removed.

A recent re-examination of the physics of tungsten inverse opals for thermal emission revealed optical properties similar to the woodpile structure can be obtained by tailoring the inverse opal structure.[32] A more open surface structure reduces the optical absorption sufficiently to permit interactions of light with the periodic structure. For this structure, modified thermal emission is therefore expected. Recently, we reported the synthesis of three-dimensionally ordered macroporous (3DOM) tungsten monoliths with external dimensions of several millimeters and an open skeletal structure that matches these theoretical requirements.[33] The 3DOM tungsten monoliths were prepared using polymer opals as template and an aqueous tungsten precursor, acetylated peroxotungstic acid (APTA). As monoliths, these porous metals could be resistively heated, producing thermal emission over relatively short time periods.

When designing a photonic crystal to work at high temperatures, several challenges must be faced, such as melting, evaporation, grain coarsening, and recrystallization of the photonic crystal. To date, tungsten has been the choice for both metallic photonic crystals and incandescent light bulbs because of the high melting temperature and low vapor pressure of this metal.[34] In tungsten wire filaments for incandescent lighting, grain coarsening and recrystallization are restrained by the addition of Al, Si, and most notably, K. With K doping in "no-sag" tungsten, K bubbles ca. 50 nm in diameter provide a stabilizing effect and reduce grain coarsening.[35] When structural dimensions are reduced from tens to hundreds of micrometers in a traditional filament to 50−100 nm in the walls of inverse opals and 1 μm in the woodpile structure, the potential for physical changes increases. At these small dimensions, higher surface-to-volume ratios of tungsten particles increase the reactivity of the metal and may lower its melting point. If the photonic crystal structure is altered as a result of thermal emission, optical properties will change. However, except for a brief mention of grain coarsening after thermal emission for 3DOM W monoliths,[33] none of the previous studies discussed the structure of the woodpile or inverse opal photonic crystal after emission.

Here, we describe the synthesis and structure of monolithic 3DOM W pieces with the relatively open skeletons necessary to reduce light absorption and evaluate the effects of heating on structural changes in various atmospheres. Effects of vapor transport and grain coarsening are observed at temperatures as low as 800 °C, but can be mitigated by alloy formation with molybdenum.

Experimental Section

The following chemicals were used as-received: methyl methacrylate (99.9%), tungsten foil (0.05 mm, 99.9+%), and tungsten monocrystalline powder (99.9+%, 0.6−1 μm) from Aldrich Chemical Co.; ammonium metatungstate hydrate (AMT) (≥99.0% as WO_3) from Fluka; ammonium molybdate tetrahydrate (AMo) (ACS grade) from Strem Chemicals; methanol (99.9%) and potassium persulfate (certified) from Fisher Scientific; glacial acetic acid (99.9%) and hydrogen peroxide (30%) from Mallinckrodt Chemicals; Ar(g) (high purity grade) and H_2(g) (industrial grade) from the University of Minnesota U-Stores; and N_2(g) from the University of Minnesota house system. Deionized water with a resistivity of 18.2 MΩ·cm was used in all aqueous syntheses. APTA was synthesized as previously described.[33]

Colloidal crystal (CC) templates were formed by slow gravity sedimentation of poly(methyl methacrylate) (PMMA) spheres, whose synthesis from methyl methacrylate with potassium persulfate as an initiator was reported previously.[36] Before infiltration, the CCs were annealed at 85 °C for 5 min.

Tungsten precursors (AMT, APTA) were dissolved in a solution of methanol:water (1:4 vol:vol) to produce 2.5−3.0 M precursor solutions. Doping of the tungsten precursor solutions with molybdenum was adapted from a procedure by Cheetham et al.[37] AMT and AMo were simultaneously dissolved in water or methanol:water (1:4 vol:vol) mixtures to form a 3.0 M metal complex solution with a nominal 95% W:5% Mo wt ratio (methanol:water as solvent) or 97% W:3% Mo wt ratio (water as solvent), based on the metal. All solutions containing AMT required the mixture to be heated to 30 °C and stirred for 60 min to dissolve the precursor salts completely. The measured Mo content was 2.8 wt % in the sample prepared from methanol:water solution and 2.6 wt % in the aqueous sample, based on ICP-mass spectrometric analyses.

For all infiltrations, CCs were evacuated in an Erlenmeyer flask with a rubber septum for a minimum of 1 h before the precursor solution was applied to the template. Precursor solutions were then dripped over the side walls of the flask using a syringe and infiltrated the evacuated CCs from the bottom up. The composite materials were dried in air and then reduced in a quartz tube under H_2 flowing at 0.5 L min^{-1} at a temperature ramped from room temperature to 800 °C at 5 °C min^{-1} with a dwell time of 1 h at the maximum temperature.

To study the thermal stability of the monolithic 3DOM W products, these were heated in a quartz tube under flowing N_2 at 0.5 L min^{-1} with a ramp rate of 10 °C min^{-1} to 500, 800, or 1000 °C and dwell times of 30 min, 1 h, or 4 h. Alternatively, they were heated resistively in one of two devices (see the Supporting Information). The first consisted of a glass jar fitted with a rubber stopper to control the atmosphere and insulate the electrical leads. The jar was purged with N_2 overnight and during emission at a rate of 0.5 L min^{-1} using syringe needles. The second device was

(28) Juarez, B. H.; Lopez, C.; Alonso, C. *J. Phys. Chem. B* **2004**, *108*, 16708−16712.
(29) Bartlett, P. N.; Ghanem, M. A.; El Hallag, I. S.; de Groot, P.; Zhukov, A. *J. Mater. Chem.* **2003**, *13*, 2596−2602.
(30) Jiang, P.; Cizeron, J.; Bertone, J. F.; Colvin, V. L. *J. Am. Chem. Soc.* **1999**, *121*, 7957−7958.
(31) von Freymann, G.; John, S.; Schulz-Dobrick, M.; Vekris, E.; Tetreault, N.; Wong, S.; Kitaev, V.; Ozin, G. A. *Appl. Phys. Lett.* **2004**, *84*, 224−226.
(32) Han, S. E.; Stein, A.; Norris, D. J. *Phys. Rev. Lett.* **2007**, *99*, 053906-1-053906-4.
(33) Denny, N. R.; Han, S.; Turgeon, R. T.; Lytle, J. C.; Norris, D. J.; Stein, A. *SPIE Proc.* **2005**, *6005*, 60050501−60050513.
(34) Lassner, E.; Schubert, W. D. *Tungsten*; Kluwer Academic: New York, 1999.
(35) Snow, D. B. *Metall. Trans. A* **1979**, *10A*, 815−821.
(36) Schroden, R. C.; Al-Daous, M.; Blanford, C. F.; Stein, A. *Chem. Mater* **2002**, *14*, 3305−3315.
(37) Cheetham, A. K.; Chowdhury, A. J. S. *J. Less-Common Met.* **1986**, *116*, 43−50.

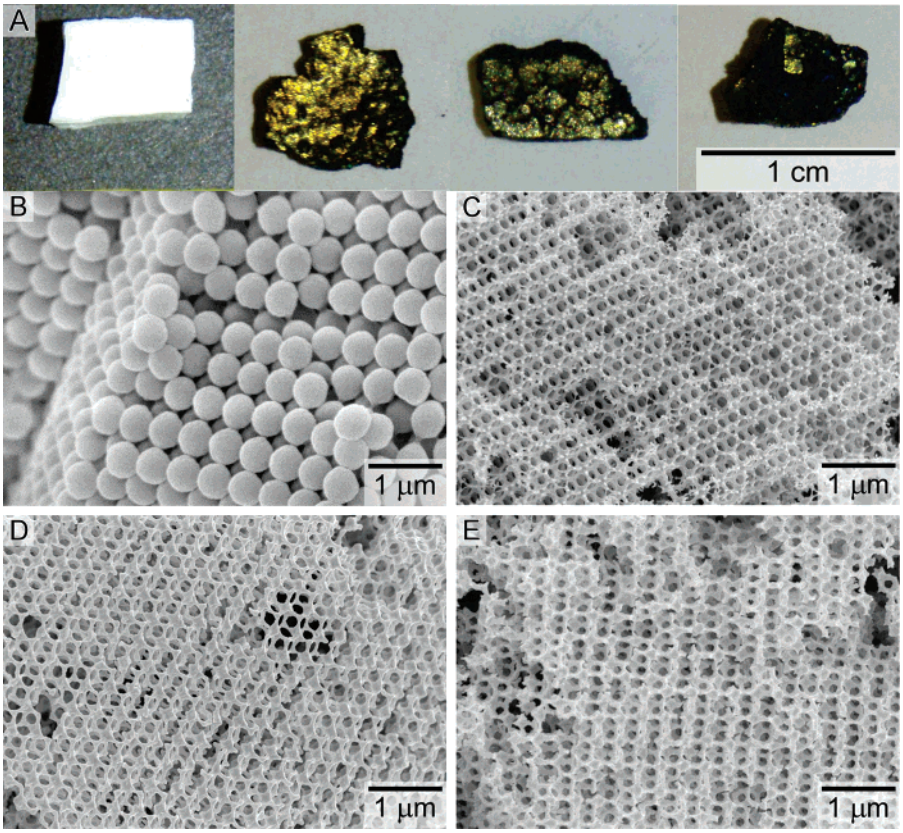

Figure 1. (A) Photographs of a PMMA colloidal crystal template, a 3DOM W monolith prepared from APTA, a 3DOM W monolith prepared from AMT, and a 3DOM WMo alloy monolith (from left to right). The scale bar applies to all four pieces. (B) SEM image of the PMMA colloidal crystal. (C) SEM image of 3DOM W prepared from APTA. (D) SEM image of 3DOM W prepared from AMT. (E) SEM image of 3DOM WMo. The SEM images reveal the differences in size and texture for the three different porous metal samples.

manufactured by MDC Vacuum Products. The main body consisted of a UHV 6-way configuration flange assembly using Del-Seal CF fittings. A medium current electrical feedthrough was used to resistively heat the samples while in the chamber. A CaF_2 window manufactured by Crystran Ltd. was used for sample observation. The UHV assembly was evacuated using a Varian Turbo V-70 pump overnight. After evacuation to 2×10^{-4} Torr, the chamber was refilled with Ar to 760 Torr. The chamber was then evacuated and refilled two additional times before emission testing to exclude as much water from the sample atmosphere as possible. In both devices, 3DOM samples were heated resistively by sandwiching the monoliths between two sets of W foil pieces to create an electrical contact and providing 10−35 W of power supplied by a Tenma CPX200 Dual 35 V 10 A power supply unit.

Scanning electron microscopy (SEM) images were obtained using a JEOL 6500 or JEOL 6700 field-emission gun SEM with an accelerating voltage of 5 kV. Sample dimensions were measured from SEM images using ImageJ software (http://rsb.info.nih.gov/ij/). Powder X-ray diffraction (XRD) patterns were obtained using a Bruker AXS microdiffractometer with a 2.2 kW sealed Cu source, Hi-Star 2-D area detector and a 0.8 mm monochromator. The diffractometer was set to 45 V and 40 A with a dwell time of 5 min per frame for data acquisition. Jade 7.0 software was employed to process the XRD patterns. For crystallite size analysis, a LaB_6 standard was used to correct for peak broadening. Metal analyses were obtained on a Thermo Elemental PQ ExCell Quadrupole ICP−MS with simultaneous detector, Meinhardt nebulizer, Peltier cooled spray chamber, and nickel cones. UV−vis reflectance spectra were acquired using a Spectral Instruments 400 Series CCD array UV−vis spectrophotometer with a W filament source and a fiber optic probe at normal incidence to the monolith surface.

For numerical calculations of reflectance spectra, a transfer matrix formalism was used in combination with a multiple scattering technique.[38] The use of the latter ensured numerical stability. A nonorthogonal mesh was used. The unit cell was described by a $18 \times 18 \times 15$ mesh. The experimentally determined dielectric function of tungsten was used, including the imaginary component (i.e., dissipation).[39] The calculation was carried out for four layers of spheres using the structural parameters listed in Table 1. The top and bottom surfaces cut through the sphere-centers of the outer layers. The transmittance was low enough in the wavelength range of interest, indicating that the optical spectra for a greater number of layers are similar.

Table 1. Structural Dimensions of 3DOM Metals Prepared from Various Precursors[a]

sample	macropore diameter (nm)	window diameter (nm)	wall thickness (nm)
3DOM W (APTA)	328 ± 21	129 ± 12	39 ± 5
3DOM W (AMT)	363 ± 25	142 ± 14	48 ± 8
3DOM WMo (H_2O)	325 ± 20	120 ± 10	54 ± 5
3DOM WMo ($MeOH/H_2O$)	335 ± 9	119 ± 11	61 ± 8

[a] Dimensions were estimated from SEM images, using ca. 25 data points per sample.

Results and Discussion

Synthesis andStructure of 3DOM W Monoliths. Figure 1A shows a photograph and Figure 1B a SEM image of a typical monolithic PMMA template. A single batch of spheres with diameters of 540 ± 9 nm was employed

(38) Bell, P. M.; Pendry, J. B.; Martin-Moreno, L.; Ward, A. J. *Comput. Phys. Commun.* **1995**, *85*, 306−322.
(39) Lynch, D. W.; Hunter, W. R. In *Handbook of Optical Constants in Solids*; Palik, E. D., Ed.; Academic Press: Orlando, FL, 1985.

throughout this study and external dimensions of the template were on the order of several millimeters (thickness ca. 3 mm). These sphere sizes were selected for synthetic convenience to investigate structural properties; larger spheres (ca. 2 μm diameters) would be chosen to examine effects of the structure on thermal emission spectra. A three-dimensionally ordered macroporous (3DOM) tungsten structure was produced by infiltrating the fcc close-packed array of PMMA spheres with a 3 M APTA solution and reducing this composite in hydrogen at 800 °C (Figure 1C). The PMMA spheres were removed during this process, and the monolithic nature and external shape of the template were translated into the product (Figure 1A). Most of the carbon from the polymer template was eliminated by this treatment, yielding a carbon content of 0.26 wt % in the product. The tungsten walls can be described as an open structure of interconnected rods around 328 ± 21 nm voids with 12 interconnecting windows at the contact points of the original polymer spheres (129 ± 12 nm window diameters) and rod thicknesses of ca. 39 ± 5 nm (see Table 1). Because of solvent loss and elimination of other precursor atoms during reduction, the pore dimensions decreased by nearly 40% compared to the template diameters. The fact that a monolith was maintained in spite of the large shrinkage implies uniform, isotropic contractions throughout the reduction process. Relatively few 3DOM structures with these large dimensions in 3D space have been prepared, other examples including 3DOM carbon and 3DOM silica.[40,41] Some local defects were observed in the structure, which are ascribed in part to imperfections in the colloidal crystal template and in part to cracks that developed during thermal processing. To minimize inhomogeneities from incomplete template infiltration, we employed a mixed-solvent system (water and methanol) that improved wetting of the PMMA spheres. In spite of the defects, periodic domains in the tungsten skeleton were large enough to produce an opalescent appearance (Figure 1A) and an optical stopband in the visible region, centered around 631 nm (Figure 2). Because of irregularities in the monolith surfaces, the stop band peak shifted slightly in wavelength and intensity when spectra were sampled at different positions. A simulated reflectance spectrum of a four-layer model with the structural parameters of this sample was qualitatively similar to the experimental spectrum. Differences from the experimental spectra resulted from approximations made in the theoretical model and from small deviations from a normal angle of incidence during measurements. Band structure calculations for this structure show that a stop gap opens from 620 to 780 nm. Therefore, the observed reflectance peak can be assigned to the stop gap along the [111] direction. A powder XRD pattern of this sample (see the Supporting Information, Figure S1) showed only reflections corresponding to α-tungsten. On the basis of line broadening in the XRD pattern, an average grain size of 19.8 ± 0.1 nm is estimated for tungsten grains in the walls of this sample.

Although tungsten monoliths derived from APTA are suitable photonic crystals for thermal emission testing, the metal-to-ligand ratio in the APTA precursor prepared by our methods can vary depending on seasonal humidity variations. Such changes can affect the product structures from batch to batch. As a precursor with stricter stoichiometry, commercially available ammonium metatungstate hydrate (AMT) was examined as the tungsten source. Products were also monolithic (Figure 1A) with an open skeletal structure similar to that of the APTA-derived samples. Shrinkage during processing was less than in the case of APTA (363 ± 25 nm void diameters) and windows were slightly larger (142 ± 14 nm), whereas the walls were thicker (48 ± 8 nm). Compared to samples derived from APTA, the products appeared less regular in SEM images with more unevenly formed rods and some instances of disconnected rods. Although these monoliths displayed opalescence, the stopband peaking at 566 nm was less pronounced than in the APTA case. Only α-tungsten was detected by XRD.

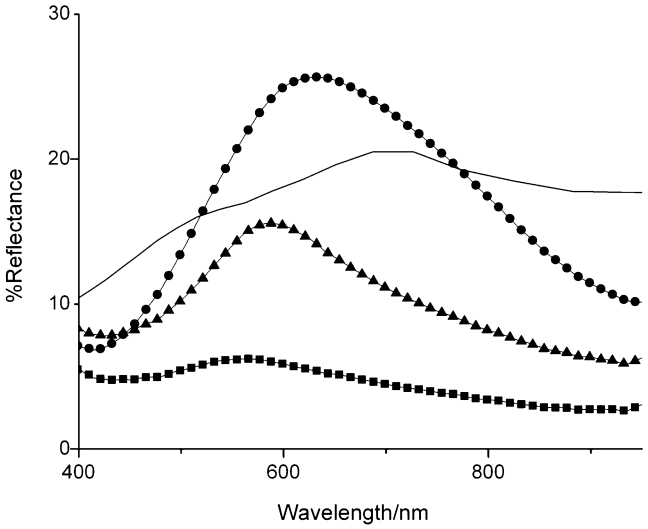

Figure 2. UV−vis reflectance spectra taken from the top surface of the monoliths depicted in Figure 1A normal to the (111) planes. Circles correspond to data for the 3DOM W sample prepared from APTA, squares to the sample prepared from AMT, and triangles to the 3DOM WMo alloy. The thin line is a simulated reflectance spectrum for 3DOM W with structural parameters corresponding to the sample prepared from APTA.

Importantly, 3DOM W products from both APTA and AMT precursors used with a PMMA colloidal crystal template displayed a much more open skeletal structure than is obtained by CVD methods[31,33] or by using certain other solution precursors, such as WCl_6.[33] Such an open structure has been predicted to lessen absorption.[32] Although the interstitial space in a colloidal crystal template is well-defined by the template geometry, morphologies of products obtained after infiltration of this space and subsequent processing can vary significantly, depending on precursor and template interactions as well as other processing details. In a previous study, we observed a wide array of morphologies, ranging from highly curved shells formed by surface templating with CVD precursors on a silica opal or with aqueous WCl_6 in a PMMA CC to more open stick structures resulting from volume templating with the aqueous precursor, APTA, in polymer colloidal crystals and intermediate morphologies with other aqueous precursors ($W(OEt)_5$).[33] Figure 3 illustrates examples of the contrasting structures. Surface templating typically results in smaller ratios of window openings to macropore diameters. Furthermore, surface

(40) Li, F.; Wang, Z.; Ergang, N. S.; Fyfe, C. A.; Stein, A. *Langmuir* **2007**, *23*, 3996−4004.
(41) Lee, K. T.; Lytle, J. C.; Ergang, N. S.; Oh, S. M.; Stein, A. *Adv. Funct. Mater.* **2005**, *15*, 547−556.

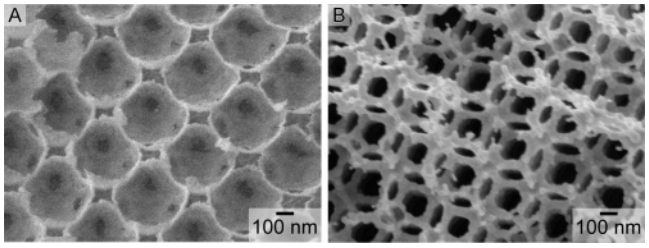

Figure 3. Illustration of the different morphologies obtained by (A) surface templating vs (B) volume templating. The SEM image in (A) shows 3DOM W prepared from a WCl_6 precursor by the method described in the literature.[33] This structure is similar to that obtained by tungsten CVD in silica colloidal crystal templates with thin metal shells conforming to the surface of the original template spheres, small interconnecting windows where spheres originally touched, and small interstitial spaces between spheres in addition to the larger macropores surrounding the air holes left by the original spheres. The SEM image in (B) corresponds to the 3DOM W sample derived from APTA shown in Figure 1C.

templating can generate interstitial holes between adjacent spheres that are not filled by the precursor. The different structures result from varying interactions between the inorganic precursor and the spherical templates during infiltration and from differences in the shrinking behavior of specific precursors during thermal processing.

Effects of Joule Heating on Structure. Because the 3DOM W samples were self-supporting and monolithic in nature with dimensions on the order of millimeters, they could be employed directly as filaments through resistive heating (Joule heating). Thermal emission testing required an inert atmosphere to avoid oxidation of the 3DOM W filaments. Two different set-ups were employed for Joule heating. The first device consisted of a glass vessel with a rubber stopper and feed-throughs for wire connections and sample purging (see the Supporting Information). The monoliths were sandwiched between two sets of W foil at each end, which also provided the electrical contact. Although this emission device did not allow for sample evacuation or rigorous exclusion of water in the sample atmosphere, it was useful for rapid qualitative measurements. When a sample of 3DOM W was resistively heated in flowing nitrogen, it began to glow brightly, illuminating the area around the sample. With many samples, emission of light could be maintained over several minutes at powers of 10−35 W. In some samples, the most intense emission wandered throughout the monolithic filament, possibly through cracks and defects in the structure. The dynamics of these "hot spots" will depend on the local conductivity, which will vary as the structural cross-section and temperature change in time. Figure 4A shows the SEM image of a sample prepared from APTA that had emitted light for 15 min with an applied power of 35 W. This filament had retained a monolithic shape but was more brittle than before Joule heating. From the SEM image, it is clear that the 3DOM structure had been lost for this sample. Instead, relatively large, micrometer-sized tungsten needles were produced in addition to globular tungsten structures resulting from grain coarsening. Prior to emission, this sample had a structure similar to that found in Figure 1C, with an average grain size of 21.3 ± 0.4 nm. After emission, the grain size was too large to be determined by XRD line broadening. The needles are a result of chemical vapor transport involving

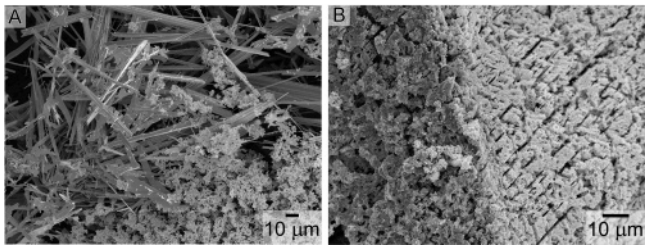

Figure 4. Typical SEM images of 3DOM W, prepared from APTA solutions (2.5 M in (A), 3.0 M in (B)), after thermal emission. (A) Product after emission at 35 W for 15 min in the first emission device. (B) Product after emission at 10W for 5 min in the second emission device.

the volatile $WO_2(OH)_2$ phase produced when hot 3DOM W reacted with residual water on its surface or in the device atmosphere (eq 1).[42]

$$W(s) + 4H_2O(g) \leftrightarrow WO_2(OH)_2(g) + 3H_2(g) \qquad (1)$$

These observations emphasize the importance of rigorously excluding water vapor from nanostructured tungsten filaments. Subsequent thermal emission studies of 3DOM W samples were therefore carried out in a testing device that could be fully evacuated. This device consisted of a metal chamber with ports to provide electrical feed-through, an observation window, and atmospheric control. After insertion of the 3DOM W sample, again sandwiched between two sets of tungsten foil, the chamber was evacuated three times to 2×10^{-4} Torr and refilled with argon each time. The sample was then resistively heated. Emission was not always uniform across the sample and the brightest spots of emission often occurred between the tungsten foil contacts on either side of the sample. Figure 4B shows a SEM image of the 3DOM W product (from APTA) after emission with an applied power of 10 W for 5 min. The lower power and shorter heating time were chosen to mitigate effects of grain coarsening. After emission, the monolithic nature of this sample was maintained but the monolith was significantly more brittle at and near the areas of emission. As seen in Figure 4B, no tungsten needles were present in this sample as a result of excluding water from the system. Nonetheless, extensive grain coarsening was still detected in areas of the sample where the brightest emission had been observed (left half of image). In regions away from these local hot spots, less change in the sample structure was apparent (right half of image).

Effects of Radiative Heating on Structure. One limitation of Joule heating in these devices was the lack of control over the emission temperature. With additional effects of local hot spots, temperatures throughout the monoliths were not uniform. To ensure a more uniform thermal history throughout the samples and evaluate the effects of temperature and heating time on grain coarsening and on the structural integrity of 3DOM W, we heated samples radiatively in quartz tubes under flowing nitrogen. Figure 5 shows SEM images of a 3DOM W sample prepared from AMT as the precursor and of this type of sample after heating in nitrogen. After heating at 500 °C, no structural change was observed after 30 min (SEM not shown). At 800 °C,

(42) Schubert, W. D. *Int. J. Refract. Met. Hard Mater.* **1990**, *9*, 178−191.

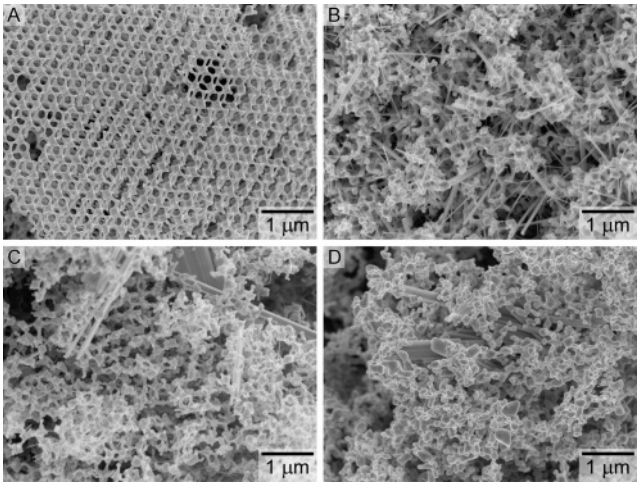

Figure 5. SEM images of 3DOM W samples prepared from AMT. (A) Sample before radiative heating. (B) Product after radiative heating in nitrogen flowing at 0.5 L min^{-1} at 800 °C for 30 min (C) Product heated at 1000 °C for 30 min (D) Product heated at 1000 °C for 1 h.

significant fractions of the 3DOM structure were maintained after 30 min, although they had fragmented into smaller domains (Figure 5B). Tungsten needles were observed in this product because water could not be completely excluded from the system, in spite of extensive purging with nitrogen. The structures of samples heated to 800 °C for 1 h (SEM not shown) and 1000 °C for 30 min (Figure 5C) were less regular and grain coarsening continued, so that after 1 h at 1000 °C, little of the original 3DOM structure was retained (Figure 5D).

These studies indicate that photonic crystals involving tungsten with features on the order of tens of nanometers are quite reactive and prone to structural changes at temperatures as low as 800 °C. The high surface-to-volume ratios in these structures facilitate surface reactions, sample evaporation, and grain coarsening. Grain growth remains an issue even when water is excluded. A promising solution to these issues was provided by alloy formation with molybdenum.

Doping of Tungsten with Molybdenum. Molybdenum doping has been noted to reduce chemical vapor transport in bulk tungsten.[42] To form photonic crystals as alloys of tungsten with molybdenum, the solvent system had to be modified. The molybdenum precursor, ammonium molybdate tetrahydrate, is less soluble in methanol:water mixtures than AMT. With 5 wt % molybdenum added to the synthesis, the molybdenum content analyzed in the product was therefore only 2.8 wt %. Switching to a purely aqueous system improved the solubility of the molybdenum precursor while still permitting infiltration of the PMMA template. In this case, 3 wt % added molybdenum yielded a product containing 2.6 wt % according to ICP-mass spectrometric analysis. Both syntheses produced well-ordered 3DOM structures whose SEM images are shown in Figures 1E and 6A, respectively. Macropore diameters and pore windows of both products were similar to those in APTA-derived products (Table 1), although walls were thicker with an average grain size of 27.9 ± 0.2 nm estimated from XRD line broadening. Because of the similarity in crystal structure of α-tungsten and molybdenum, no distinct peaks were detected for the molybdenum component. The alloy monoliths were visibly opalescent (Figure 1A) and produced a well-defined stopband centered around 586 nm, which attests to the structural order, in particular at the surface of the monoliths.

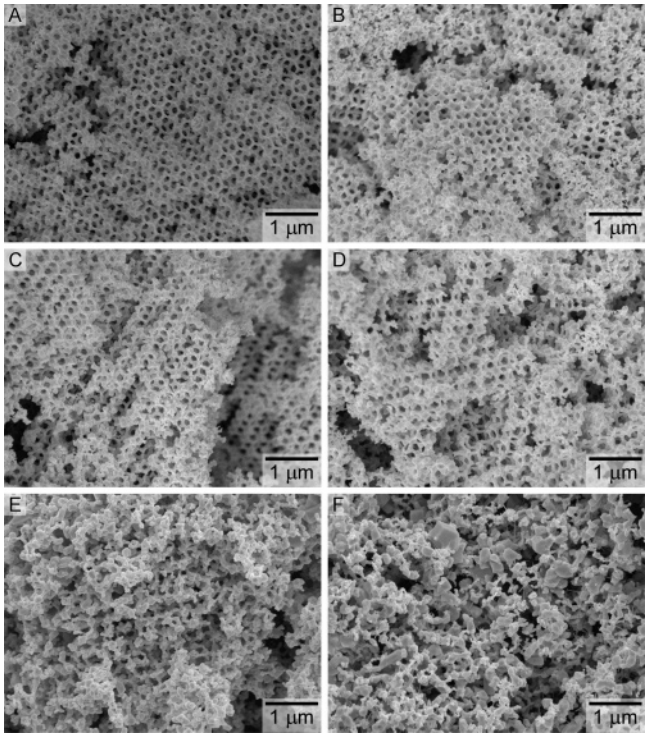

Figure 6. SEM images of 3DOM WMo alloys. (A) Sample before radiative heating. (B) Product after radiative heating in nitrogen flowing at 0.5 L min^{-1} at 800 °C for 30 min (C) Product heated at 800 °C for 1 h. (D) Product heated at 800 °C for 4 h. (E) Product heated at 1000 °C for 30 min (F) Product heated at 1000 °C for 1 h. Samples A−D were originally prepared using only H_2O as the solvent, E and F using methanol/water solvent mixtures.

Table 2. Average Metal Grain Sizes before and after Thermal Treatments of 3DOM WMo[a]

heating temperature (°C)	initial size (nm)	after 30 min (nm)	after 1 h (nm)	after 4 h (nm)
800	27.9 ± 0.2	27.4 ± 0.3	30.9 ± 0.3	29.6 ± 0.2
1000	28.7 ± 0.2	41.5 ± 0.3	49.0 ± 0.5	not determined

[a] Grain sizes were determined from line broadening in XRD powder patterns. Samples heated to 800 °C were originally prepared using only H_2O as the solvent; samples heated to 1000 °C were prepared using methanol/water solvent mixtures.

The effects of radiative heating on 3DOM WMo alloys are shown in the SEM images of Figure 6. It is notable that needles were absent from all samples, except for a few very small needles in the sample heated at 1000 °C for 1 h, indicating that molybdenum does in fact mitigate chemical vapor transport reactions. Furthermore, the 3DOM structure was maintained in these alloys even after heating at 800 °C for 4 h. Grain sizes estimated from XRD line broadening remained approximately constant during this treatment (Table 2). After heat treatment at 1000 °C for 30 min, some sintering was observed, but the change was significantly less than in the molybdenum-free samples. After 1 h at 1000 °C, grain coarsening became significant.

Conclusion

A wet chemical synthesis using the water-soluble tungsten precursors APTA and AMT with PMMA colloidal crystal

templates produced monolithic 3DOM tungsten pieces with millimeter dimensions in all three dimensions. The skeletal structures were much more open than those of tungsten inverse opals prepared by chemical vapor deposition or from aqueous WCl_6 precursors and should therefore reduce optical absorptions by the tungsten framework that has prevented the observation of strong photonic crystal effects in previous studies of tungsten inverse opals. The order in these materials extends over limited domains, but in metallic photonic crystals, these are large enough to observe stop bands in the UV−visible spectra. As free-standing monolithic structures, these 3DOM W samples can be resistively heated to evaluate thermal emission without the need of an underlying support. Because of their small structural dimensions and relatively large interfacial areas, the heated materials readily react with trace amounts of water, leading to tungsten needle formation by chemical vapor transport, which is believed to involve the well-known volatile $WO_2(OH)_2$ phase. In addition, grain growth occurring during Joule heating or radiative heating of the 3DOM W samples at temperatures as low as 800 °C can destroy the periodic structure of the photonic crystal, which would lead to deterioration of its photonic properties. It should be noted again that in these investigations, PMMA spheres with diameters of 540 nm were used as templates mainly for synthetic convenience. Metallic photonic crystals designed to modify emission in the infrared region of the spectrum would require larger macropores templated from larger spheres (ca. 2 μm diameters). The resulting structures would have slightly larger wall thicknesses, which may reduce structural changes to some degree. However, a more reliable means of maintaining structural integrity during heat treatments was found by alloying 3DOM W with ca. 3 wt % Mo. Alloy formation effectively suppressed needle formation during heat treatment, even when trace water was present in the surrounding atmosphere. Furthermore, it significantly decreased grain growth at 800 °C, so that the 3DOM structure could be maintained at this temperature for at least 4 h. Again, this stabilizing effect should be greater for tungsten photonic crystals with larger structural features and smaller specific surface areas. The combined advances described in this study, formation of a monolithic refractory metal with a periodic macroporous structure on an optical length scale, production of a relatively open structure, and thermal stabilization by alloy formation, provide important new opportunities for the design of metallic photonic crystals for thermal emission control. We are now beginning spectral measurements to quantify the influence of structure on thermal emission of templated tungsten photonic crystals.

Acknowledgment. This work was supported by the U.S. Department of Energy (DE-FG02-06ER46348) using resources at the University of Minnesota Characterization Facility, which is supported by the MRSEC program of the NSF (DMR-0212302). We thank Rick Knurr at the University of Minnesota Department of Geology and Geophysics for the ICP−MS analyses. S.E.H. and D.J.N. acknowledge fellowships from the Samsung and Alexander von Humboldt Foundations, respectively.

Supporting Information Available: Powder XRD patterns of the 3DOM metals, photographs of the thermal emission testing chambers, and a calculated band diagram for the 3DOM W sample prepared from APTA (PDF). This material is available free of charge via the Internet at http://pubs.acs.org.

CM071228P